Physicochem. Probl. Miner. Process., 60(4), 2024, 192417

http://www.journalssystem.com/ppmp

Physicochemical Problems of Mineral Processing

ISSN 1643-1049

Research on separation mechanism of coal gangue photoelectric sorting recognition

Wei Zhou, Haoyu Wang, Lingling Wang, Anan Feng, Liansheng Li, Jinbo Zhu

School of Materials Science and Engineering, Anhui University of Science and Technology, Huainan 232001, China

Corresponding author: Haoyu Wang (hywang2000@162.com)

Abstract: Efficiently realizing the separation of coal gangue is a hot issue in coal preparation. To solve this problem, this paper proposes research on the identification and separation of minerals in coal gangue based on dual-energy X-rays, and conducts experimental research on four single minerals and several different composite minerals in coal based on the identification technology in the sorting process of the system, and conducts a simulation study on the jet separation simulation for the separation technology in the separation process of the system. Based on the coal gangue photoelectric separation test platform, the main minerals in coal gangue were analyzed. Based on MATLAB software, the grey value of the mineral was obtained, the curve between the grey value and the thickness was made, the mass absorption coefficient of the mineral in the high and low energy regions was obtained by regression analysis, and the R value identification threshold of single mineral and composite mineral was established, which provided a theoretical basis for the accurate identification of coal gangue. The parameters of the jet nozzle were analyzed and optimized through fluid simulation, and the optimal parameters for the rapid separation of coal gangue were determined.

***Keywords*:** gangue identification, gangue separation, X-ray, mass absorption coefficient, R-value identification, jet nozzle

1. Introduction

With the rapid growth of China's economy, the people's demand for the existing standard of living is getting higher and higher, and the energy demand continues to increase, while the technology of new energy sources has not yet matured, it can be seen that coal will remain one of the world's most important sources of energy (Huang, 2018; Liu and Liu, 2018; Hou, 2019).

How to select coal with high efficiency and low pollution has become an object of increasing global concern (Zhai, 2019; Zhang, 2016; Li, 2019). Compared with the traditional wet coal separation, the gangue photoelectric separation has the great advantage of more energy saving and environmental protection, at the same time, the gangue photoelectric separation technology is constantly developing, and gradually become a hot spot in the coal selection industry. The key to coal gangue photoelectric separation is the identification and separation of coal gangue, the technology is mainly the use of X-rays for identification, and the use of jet blowing for the separation of coal gangue. X-ray penetration of the material attenuation law with the change of the density of the material itself changes, the true density of coal is about 1.3-1.5, the main impurity gangue in the coal of the true density of the main impurity gangue of about 1.7-1.9, so that it can be derived from the density of the coal and coal gangue There is a big difference between coal and gangue (Li and Zhang, 1995; Ma and Jiang, 2004; Huang et al.,2020). According to the unique nature of X-ray, the use of its detection of coal and gangue gets through the coal and gangue after the X-ray image, and then into the coal gangue separation part, relying on the blowing separation device to realize the coal and gangue sorting (Guo et al., 2021; Mei, 2023).

In recent years, many scholars have carried out a lot of research on the recognition and separation of gangue photoelectricity, and have achieved considerable results. Based on the application of dual-energy X-ray technology on security equipment, the research team of Yuan proposed the method of obtaining the area absorption coefficient of the transmitted signal through the complexification of

DOI: 10.37190/ppmp/192417

Simpson's formula for the identification of different substances, which is effective (Yuan and Sun, 2006). Duan established a mathematical model between X-ray tube voltage, greyscale, and thickness, and proposed a variable energy X-ray line scanning imaging method for the effect of thickness, by adjusting the tube voltage value of the X-ray line source to correct the effect caused by the thickness of the object to be examined (Duan, 2010). To test the sorting of different minerals, the design of dual-energy X-ray detectors, optical cameras electromagnetic sensors, and other technologies used in conjunction to obtain a variety of specialties of different materials, and this technology has been applied to practical industrial applications. Based on the dual-energy X-rays in the high-energy and low-energy material transmission signal analysis, Swedish scholars Norlin through the high- and low-energy transmission signals of the integral ratio difference to achieve the realization of the effective atomic number of the material to determine the method (B. Norlin et al., 2004). Spanish scholars Picon et al. have studied the images of crushed metals in high-energy X-ray transmission to identify non-ferrous metals, such as copper and aluminum, to spatial feature discrimination fuzzy recognition, and other image processing techniques. (Artzai et al., 2010). The development of using X-rays to identify gangue and other minerals has been more recently developed in recent years. In the simulation test to study the X-ray gangue recognition technology, the acquisition of mineral images with MATLAB software has become a research hotspot, Pan et al. based on the MATLAB software for mineral image processing, obtained the grey value of different minerals, and through the statistical analysis of the test data to find out the recognition threshold between different minerals (Pan et al., 2017). In the process of jet separation of gangue, it is a prerequisite to study the array nozzle jet performance. After the response of the electromagnetic valve, the air pressure is jetted out from the nozzle, impacting the separation target in the fallout, realizing the separation of fine coal and gangue. This process requires the selection of appropriate nozzle structure parameters that can meet the separation requirements and consume less energy. Yu et al. through CFD(Computational Fluid Dynamics) simulation software, for streamlined nozzle, from the jet velocity, jet core section length and gas consumption and other aspects of the total length of the nozzle, the length of the contraction section, the exit diameter and the contraction ratio and other factors on the impact of the nozzle jet, a comprehensive consideration, when the total nozzle length of 25 mm, the contraction section length of 4 mm, the exit diameter of 5 mm, the contraction ratio of 1.6, the nozzle jet when the total length of the nozzle is 25 mm, the length of the shrinkage section is 4 mm, the diameter of the outlet is 5 mm, and the shrinkage ratio is 1.6, the nozzle jet performance is relatively good and the air consumption is low (Yu et al., 2019). Hu et al. determined the separation standard and minimum input pressure of sorted plastics by analyzing the force of sorted plastics and carried out tests on the influence of nozzle diameter and tube length on the output pressure and nozzle jetting range and layout test, the results show that: the output pressure is positively correlated with the nozzle diameter, and the tube length shows positive correlation and then negative correlation phenomenon, and considering the overall situation, the radius is 3.5 mm, the length of the tube is 60 mm, and the distance of the adjacent nozzles is 45 mm jet effect is the best (Hu et al., 2013). Based on the theory of aerodynamics and rock mechanics, Song et al. found that air jet coal breaking is a continuous integrated process of high-pressure gas accelerated from the nozzle and developed in the air medium until the impact of coal breaking, with different characteristics and control mechanisms at different stages, and through the establishment of a mathematical model of the whole process of air jet impact coal breaking, the theoretical derivation of the air jet coal breaking capacity and crushing crater characteristics of the identification guidelines for further theoretical research and It lays the foundation for further theoretical research and on-site process design. (Song et al., 2020; Stańczyk, 2020; Li et al., 2013; Li et al., 2011). Domestic and foreign scholars focus on the image algorithm of coal and gangue quite a lot of research, but in the relationship between the nature of coal and gangue and the X-ray attenuation law is still little research.

Based on previous research, this paper explores four single minerals and several different composite minerals' grey value, establishes the relationship model between grey value and single mineral density and thickness, fits the gangue mass absorption coefficient, and establishes the R-value identification threshold, so as to explore the influence law of different minerals gangue on dual-energy X-rays. The jet separation nozzle is simulated through fluid simulation to optimize its parameters. In this work, the identification process and separation mechanism of different composite minerals in coal based on dual-energy X-rays are mainly studied experimentally.

2. Response law of coal gangue with different mineral components to X-rays

2.1. Test systems and methods

2.1.1. Instruments and test systems

The test system is mainly divided into four parts, as shown in Fig. 1, where 1 is the feeding mechanism, 2 is the conveying mechanism, 3 is the recognition mechanism, and 4 is the sorting mechanism. The research mainly focuses on the recognition mechanism and sorting mechanism, 3 is the recognition mechanism of the test system, the gangue material through the X-ray, X-ray will appear different degrees of attenuation, the recognition system will collect the sample image, each sample has a low-energy region and high-energy region of the two images, the collected images are usually processed with MATLAB software, set the grey value command to process the image to get the mineral in the high and high energy regions, the grey histogram, according to the different energy regions, the energy region and the energy region, and the energy region of the mineral in the high and high energy regions. The grey scale histogram in the high energy zone and high energy zone, according to the grey scale histogram of different energy zones can get the greyscale peak, and the greyscale peak characterizes the influence of different mineral components of the gangue after being penetrated by X-rays. 4 is the sorting mechanism, relying on the jet blowing separation device to achieve accurate separation of coal gangue, simulation of the jet nozzle to optimize its structural parameters, to achieve accurate and low energy consumption jet separation.

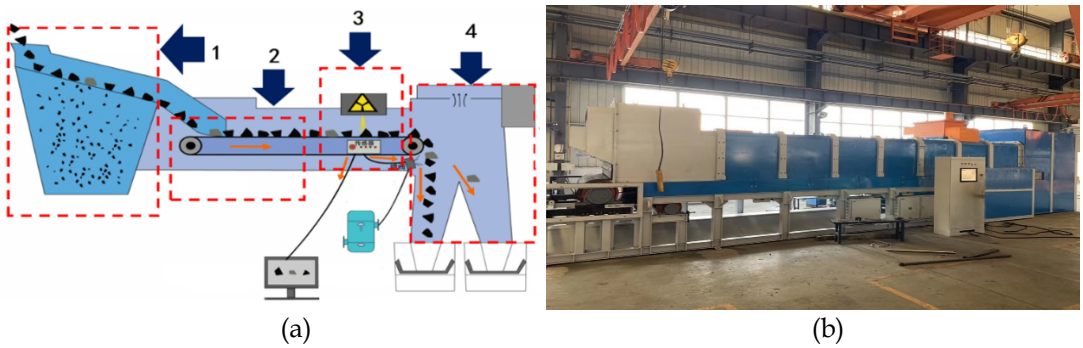

(a) (b)

Fig. 1. Test system structure diagram. (a) Test system structure; (b) Physical diagram of the test system

2.1.2. Test sample

In order to investigate the response of different mineral components of gangue to X-rays, four single minerals and different composite mineral samples were made for the test, of which, four single minerals as the control, and different composite minerals represent different mineral components of gangue. The four single minerals are graphite, quartz, kaolin, and montmorillonite, according to the requirements of the minerals by the same density compaction to 4.0mm, 4.5mm, 5.0mm, 5.5mm, 6.0mm, 6.5mm, 7.0mm, 7.7mm, eight different thicknesses, and each thickness of each do 1~2 pressure piece.

The mass ratios of the two composite minerals (graphite: quartz/kaolin/montmorillonite) were 6:1, 5:1, 4:1, 3:1, 2:1, and 1:1, with the same mass, thickness, and density in each ratio. The mass ratios of the three composite minerals (graphite, quartz, and kaolinite/montmorillonite, graphite, kaolinite, and montmorillonite) are 6:1:1, 5:1:1, 4:1:1, 3:1:1, 2:1:1, 1:1:1, and the four composite minerals (graphite, quartz, kaolinite, and montmorillonite) are 6:1:1:1, 5:1:1:1, 4:1:1:1, 3:1:1:1, 2:1:1:1:1, and 1:1:1:1, again with the same mass, thickness, and density at each ratio. The specific compositions are shown in Table 1.

2.2. Analysis of test results

2.2.1. Mineral grey value distribution

The imaging characteristics of different minerals in coal in the high and low energy regions are shown in Fig. 2~5.

Comprehensive analysis of X-ray dynamic images of different minerals in Figs. 2~5 shows that minerals with different thicknesses have different degrees of attenuation to X-rays, and there is a certain gap between the image features presented by different minerals under the condition of the

same thickness, however, this gap is difficult to be analyzed accurately from the pictures, in order to accurately differentiate between the different minerals, and therefore, it can be considered that the information on the pictures can be presented in another easier-to-differentiate In order to accurately distinguish the differences between different minerals, it can be considered to express the information on the pictures in another form that is easier to distinguish.

The peak grey levels of a single mineral in the high and low energy regions are plotted as shown in Fig. 6.

Table 1. Sample composition table of composite minerals

Two composite minerals				Three composite minerals				Four Complex Minerals			
Quality ratio	Quality (g)	Thick-nesses (mm)	Densi-ties (kg/L)	Quality ratio	Quality (g)	Thick-nesses (mm)	Densi-ties (kg/L)	Quality ratio	Quality (g)	Thick-nesses (mm)	Densi-ties (kg/L)
6:1	10.50	3.00	2.19	6:1:1	12.00	3.60	2.083	6:1:1:1	13.50	3.50	2.41
5:1	10.80	3.10	2.18	5:1:1	12.60	3.80	2.07	5:1:1:1	14.40	3.80	2.37
4:1	11.20	3.20	2.20	4:1:1	13.50	4.00	2.11	4:1:1:1	15.75	4.50	2.19
3:1	12.00	3.50	2.14	3:1:1	15.00	4.20	2.23	3:1:1:1	18.00	5.50	2.05
2:1	13.50	4.00	2.11	2:1:1	18.00	5.50	2.05	2:1:1:1	22.50	7.00	2.01
1:1	18.00	5.50	2.05	1:1:1	27.00	9.00	1.88	1:1:1:1	36.00	11.80	1.91

(a) (b)

Fig. 2. X-ray dynamic images of graphite with different thickness. (a) Low energy region; (b) High energy region

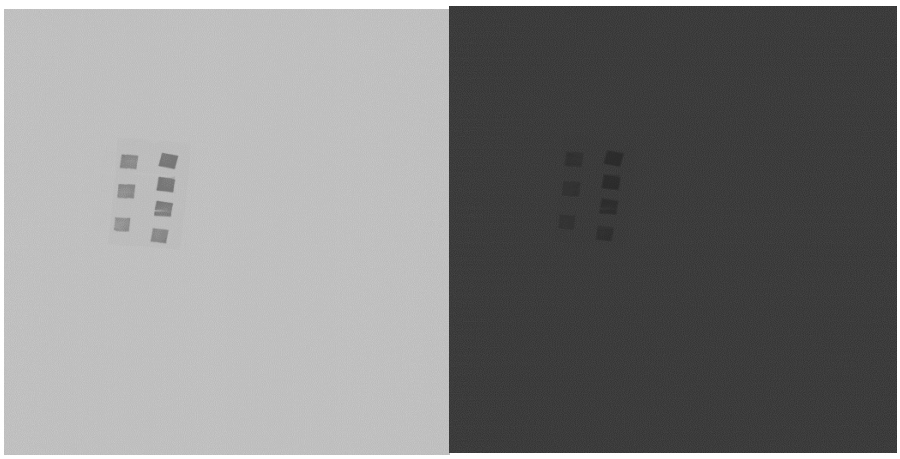

(a) (b)

Fig. 3. X-ray dynamic images of quartz with different thickness grades. (a) Low energy region; (b) High energy region

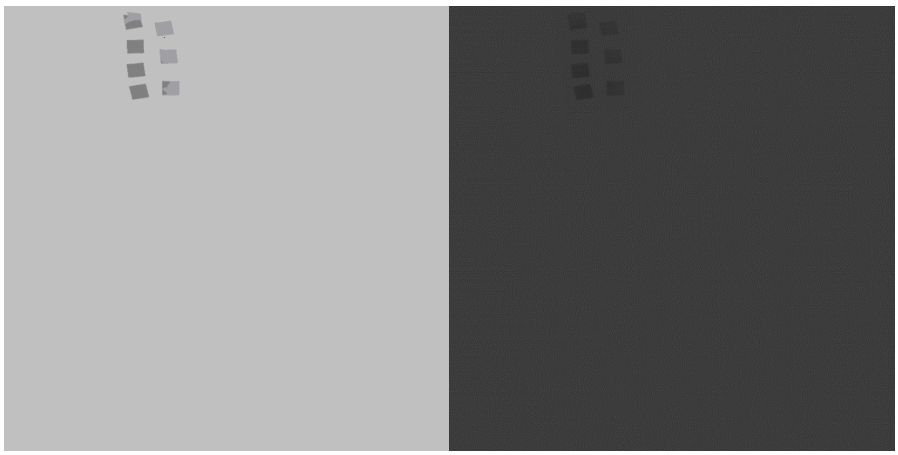

(a) (b)

Fig. 4. X-ray dynamic images of kaolin with different thickness grades. (a) Low energy region; (b) High energy region

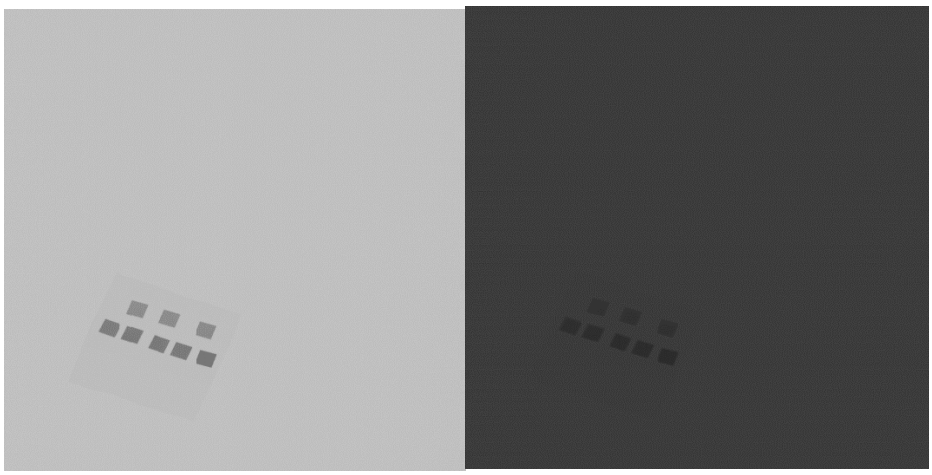

(a) (b)

Fig. 5. X-ray dynamic images of montmorillonite with different thickness grades. (a) Low energy region; (b) High energy region

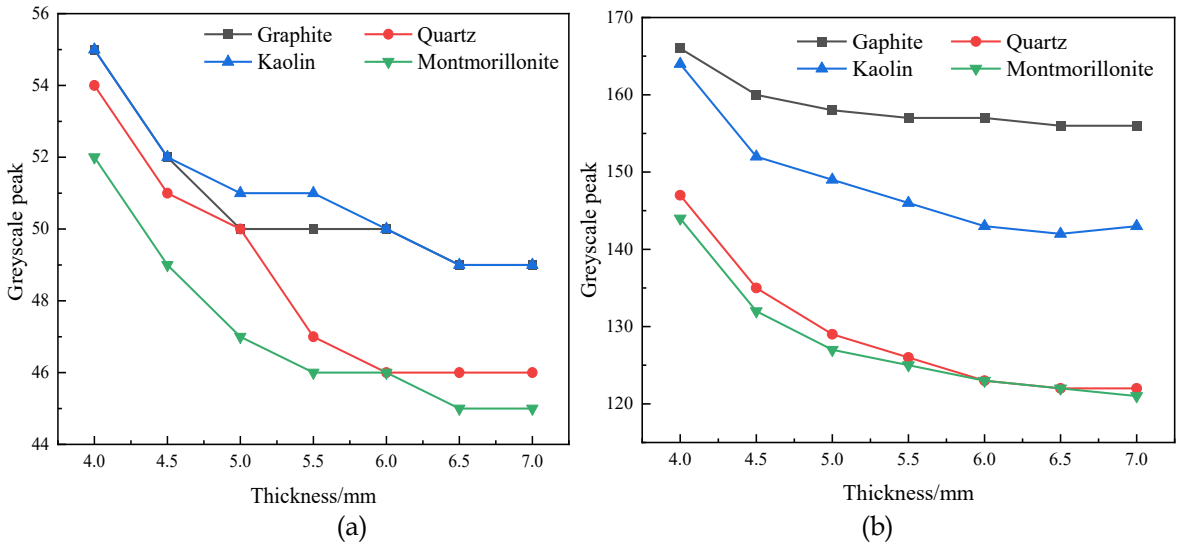

(a) (b)

Fig. 6. Relationship curves between peak greyness and thickness for four single minerals. (a) Low energy zone; (b) High energy zone

In the analysis of the peak grey values of several composite minerals, the peak grey curves obtained for a clearer analysis of the relationship between the peak grey values and the thickness of the composite minerals are shown in Figs. 7, 8, and 9. As shown in those Figs., after comparing the greyness peaks in the same energy region, it is found that the greyness peaks decrease with the increase of the sample thickness, which confirms that the attenuation degree of X-rays is negatively correlated with the thickness of the sample and positively correlated with the density of the sample. Comparison of the peak grey values of different composite minerals reveals that the greater the proportion of clay minerals in the composite minerals, the higher the peak grey value of the minerals. Single minerals and composite minerals grey peak and thickness change into a certain linear relationship between the integrated grey value with the thickness of the decreasing trend, and the degree of attenuation of X-rays is similar.

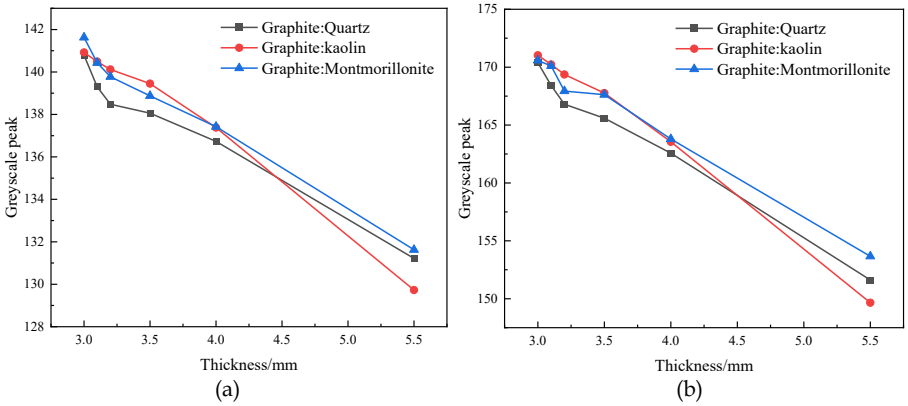

Fig. 7. Relationship curves between peak greyness and thickness of two composite minerals. (a) Low energy zone; (b) High energy zone

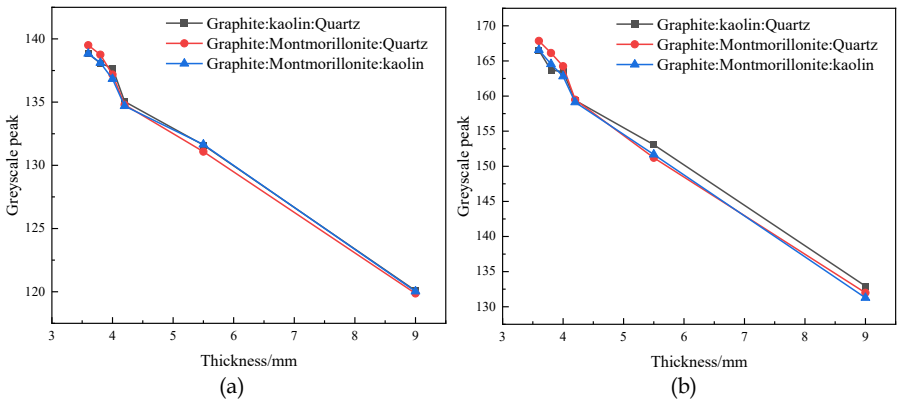

Fig. 8. Relationship curves between peak greyness and thickness for three composite minerals. (a) Low energy zone; (b) High energy zone

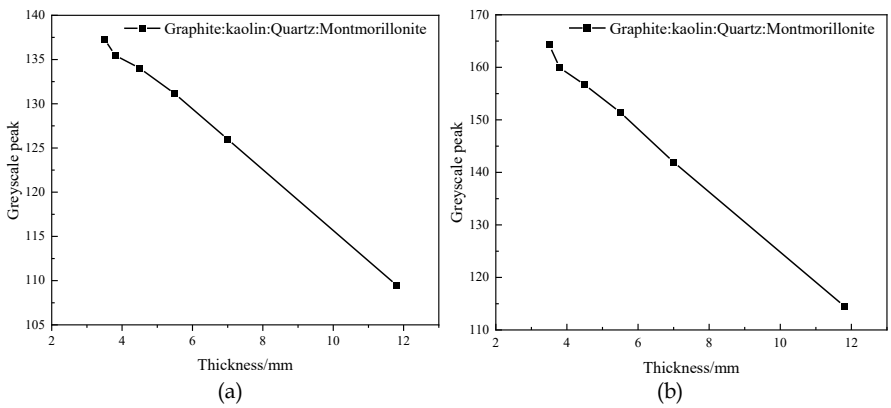

Fig. 9. Relationship curves between peak greyness and thickness for four composite minerals. (a) Low energy zone; (b) High energy zone

2.2.2. Mineral mass absorption coefficient

The relationship between the peak grey value of the minerals and the thickness and density conforms to the exponential empirical formula, from which it can be fitted by using the regression equation, considering that the thickness affects the variation of the peak grey value, it can be considered that the relationship between the thickness and the peak grey value is a binary non-linear relationship (Yi, 2022). Considering the ease of calculation, the curve will be fitted in this work using the density level fixed and the grey value versus thickness. If the relationship between grey value and thickness of graphite is used, the graphite thickness can be set as x and the peak grey value as y. The empirical equation can be expressed as:

$$y = a \cdot e^{bx} \tag{1}$$

Taking logarithms on both sides at the same time gives:

$$\ln(y) = \ln(a) + bx \tag{2}$$

From the graphite in the high-energy region and the low-energy region of the peak grey level is easy to know graphite in the high-energy region of the peak grey level - thickness linear regression calculation table, as shown in Table 2. According to the calculation of Table 2, L_{xx}、L_{xy}、L_{yy} can be obtained:

- $L_{xx} = \sum_{i=1}^{n}(x_i - \bar{x})^2 = \sum_{i=1}^{n} {x_i}^2 - n \cdot (\bar{x})^2 = 275.00 - 8 \times 5.75^2 = 10.50$
- $L_{xy} = \sum_{i=1}^{n}(x_i - \bar{x})(y_i - \bar{y}) = \sum_{i=1}^{n} x_i \cdot y_i - n \cdot \bar{x} \cdot \bar{y} = 232.9467 - 8 \times 5.75 \times 5.0679 = -0.1767$
- $L_{xx} = \sum_{i=1}^{n}(y_i - y)^2 = \sum_{i=1}^{n} {y_i}^2 - n \cdot (\bar{y})^2 = 205.4727 - 8 \times 5.0679^2 = 0.0032$

Table 2. Calculation table of grey peak thickness regression analysis of graphite high energy region

Project / number	x_i	y_i	x_i^2	y_i^2	$x_i y_i$
	x	$\ln(y)$			
1	4.0	5.1120	16.0000	26.1324	20.4480
2	4.5	5.0876	20.2500	25.8836	22.8942
3	5.0	5.0752	25.0000	25.7574	25.3759
4	5.5	5.0626	30.2500	25.6299	27.8443
5	6.0	5.0562	36.0000	25.5656	30.3375
6	6.5	5.0499	42.2500	25.5010	32.8241
7	7.0	5.0499	49.0000	25.5010	35.3490
8	7.5	5.0499	56.2500	25.5010	37.8739
$\sum_{i=1}^{8}$	46.0	40.5432	275.0000	205.4721	232.9467
$\frac{1}{8}\sum_{i=1}^{8}$	5.75	5.0679	34.3750	25.6840	29.1183

Calculate the coefficients of the regression equation:

- $b = \frac{L_{xy}}{L_{xx}} = \frac{-0.1767}{10.5} = -0.0168$
- $\ln(a) = \bar{y} - b\bar{x} = 5.0679 + 0.0168 \times 5.75 = 5.1645$
- $a = e^{\ln(a)} = e^{5.1645} = 174.95$

Thus, a regression equation can be obtained between the peak grey level and thickness of graphite in the high energy region: $y = 174.95e^{-0.0168x}$

Regression equation correlation coefficient test:

$$y = \frac{L_{xy}}{\sqrt{L_{xx} \cdot L_{yy}}} = \frac{-0.1767}{\sqrt{10.5 \times 0.0032}} = -0.9614$$

Querying the critical table of correlation coefficients, when n = 8, the degree of freedom f = n - 2 = 6, $\gamma_{a,n-2} = \gamma_{0.05,6} = 0.7067$, $\gamma \geq \gamma_{0.01,6}$, which indicates that the greyness value of graphite has a high linear relationship with the thickness, and is negative, indicating that the greyness value of graphite is negatively correlated with the thickness. This shows that the grey value of graphite is positively correlated with the thickness under the condition of certain control density, which is consistent with the above analysis. The regression equations and linear correlation coefficients between the peak grey values and thickness of graphite, quartz, kaolinite and montmorillonite in the high-energy and low-energy zones, respectively, can be obtained in accordance with the above calculations. Composite minerals can be fitted by regression analysis with the same consideration. Since the density of composite minerals at different mass ratios is similar, the density classes can be fixed and the curves can be fitted in terms of thickness versus greyness values. The regression equations for the mineral grey values are shown in Table 3.

Table 3. Grey value regression equation of four single minerals

Project / Minerals	Regression equation		Correlation coefficient	
	Low energy	High energy	Low energy	High energy
Graphite	$y = 174.95e^{-0.0168x}$	$y = 59.25e^{-0.0279x}$	-0.9614	-0.9595
Quartz	$y = 177.31e^{-0.0580x}$	$y = 65.69e^{-0.0552x}$	-0.9606	-0.9660
Kaolin	$y = 186.95e^{-0.0442x}$	$y = 61.61e^{-0.0345x}$	-0.9529	-0.8627
Montmorillonite	$y = 161.80e^{-0.0426x}$	$y = 58.02e^{-0.0373x}$	-0.8799	-0.8745
Graphite: Quartz	$y = 193e^{-0.0441x}$	$y = 151.12e^{-0.0256x}$	0.9949	-0.9888
Graphite: Kaolin	$y = 201.34e^{-0.0534x}$	$y = 156.00e^{-0.0331x}$	0.9968	-0.9939
Graphite: Montmorillonite	$y = 192.93e^{-0.0412x}$	$y = 153.13e^{-0.0275x}$	0.9957	-0.9945
Graphite: Montmorillonite: Quartz	$y = 191.26e^{-0.0405x}$	$y = 152.43e^{-0.0266x}$	0.9967	-0.9959
Graphite: Kaolin: Quartz	$y = 194.68e^{-0.0438x}$	$y = 152.98e^{-0.0274x}$	0.9929	-0.9926
Graphite: Montmorillonite: Kaolin	$y = 193.08e^{-0.0432x}$	$y = 151.98e^{-0.0263x}$	-0.9969	-0.9951
Graphite: Quartz: Montmorillonite: Kaolin	$y = 190.10e^{-0.0426x}$	$y = 151.2421e^{-0.0270x}$	-0.9987	-0.9979

As can be seen from Table 3, the thicknesses of graphite, quartz, kaolin and montmorillonite show a good negative correlation with the greyness values under the same density conditions, and this relationship is independent of the types of minerals, i.e., any minerals in the coal can be expressed by this empirical equation. The thicknesses of the composite minerals show a good negative correlation with the greyness values, and this relationship is independent of the types of minerals in the composite minerals, i.e. any mineral in the coal can be expressed by this empirical equation regardless of the composite of several minerals.

The peak grey value of minerals and the thickness of minerals meet the exponential empirical formula, let set the thickness of minerals as x, the peak grey value as y, the empirical equation can be expressed as , based on the Lambert-Beer law: , it can be concluded that the coefficient b in the regression equation can be replaced with the linear absorption coefficient μ in the formula, and because the linear absorption coefficient is directly proportional to the density: $\mu_m = \mu / \rho$, therefore, the ratio of linear absorption coefficient and average density can be called the mass absorption coefficient μ_m, thus the average mass absorption coefficient of different minerals in the coal can be obtained. The ratio of the linear absorption coefficient to the average density can be called the mass absorption coefficient μ_m,

from which the average mass absorption coefficients of the different minerals in the coal can be obtained.

The linear absorption coefficient and mass absorption coefficient of composite minerals show a good linear relationship, and the ratio of linear absorption coefficient and mass absorption coefficient is density, so under the condition that the density is known, the mass absorption coefficient of composite minerals can be obtained by their linear absorption coefficients.

The mass absorption coefficients of single minerals and composite minerals are shown in Table 4.

Table 4. Mass absorption coefficient of mineral

Performances / Minerals	Average density kg/L	Linear absorption coefficient		Mass absorption coefficient	
		Low energy zone	High energy zone	Low energy zone	High energy zone
Graphite	1.77	0.0168	0.0279	0.0095	0.0158
Quartz	1.86	0.0580	0.0552	0.0312	0.0297
Kaolin	1.51	0.0422	0.0345	0.0279	0.0228
Montmorillonite	1.81	0.0426	0.0373	0.0235	0.0206
Graphite: Quartz	2.1433	0.0441	0.0256	0.0206	0.0119
Graphite: Kaolin	2.1433	0.0534	0.0331	0.0249	0.0154
Graphite: Montmorillonite	2.1433	0.0412	0.0275	0.0192	0.0128
Graphite: Quartz: Montmorillonite	2.0696	0.0405	0.0266	0.0196	0.0129
Graphite: Quartz: Kaolin	2.0696	0.0438	0.0274	0.0212	0.0132
Graphite: Montmorillonite: Kaolin	2.0696	0.0432	0.0263	0.0209	0.0127
Graphite: Quartz: Montmorillonite: Kaolin	2.1546	0.0426	0.0270	0.0198	0.0125

As shown in Table 4, the mass absorption coefficient of graphite is much smaller than the mass absorption coefficients of other minerals in coal, while the mass absorption coefficients of composite minerals are larger than those of graphite and smaller than those of quartz, kaolin and montmorillonite. According to the composition of minerals, based on the equivalent atomic number, the equivalent atomic number of graphite is much smaller than other minerals, so the mass absorption coefficient of graphite is much smaller than the mass absorption coefficient of other minerals in coal, so it can be deduced that the mass absorption coefficient of coal is smaller than the mass absorption coefficient of gangue, and it is based on the differences in mass absorption coefficients between the coal and gangue that makes it possible for the use of X-rays to recognize coal and gangue to become a reality.

The experimental analysis shows that the grey value decreases with the increase in the thickness of the minerals and based on the grey value curves, the grey value of different minerals shows a good exponential relationship with the thickness as analyzed by the regression equation idea. In the regression equation study of different minerals, there is a linear relationship between linear absorption coefficient and mass absorption coefficient. If the linear absorption coefficient is used to model the decay of grey value of different minerals, the regression equation will be complicated and variable. On the other hand, the mass absorption coefficient is the most basic property of the embodied substance, which is only related to its own equivalent atomic number, so the use of mass absorption coefficient to establish the attenuation model of the grey value of the raw coal is more standardized and normalized. Therefore, the formula for the decay of ray intensity can be expressed as $I = I_0 e^{\mu_m \rho d}$. According to the average mass absorption coefficient of different minerals, the grey value regression equation can be rewritten to obtain the grey value attenuation model of different minerals, as shown in Table 5.

For different kinds of coal, they contain different mineral compositions, which are mainly represented as graphite, quartz, kaolin, montmorillonite and calcite, etc. In this work, graphite, quartz, kaolin and montmorillonite are used in the composite respectively, which can be regarded as different kinds of coal. From the attenuation model of composite minerals, it can be seen that different kinds of coal can also be represented by this model. In the process of actual coal beneficiation, the mass absorption coefficient of coal can be determined and can be measured by instruments, so based on the

Table 5. Attenuation model of grey value of four single minerals

Minerals \ Project	Low energy	High energy
Graphite	$y = 175e^{-0.0095dx}$	$y = 59e^{-0.0158dx}$
Quartz	$y = 177e^{-0.0312dx}$	$y = 66e^{-0.0297dx}$
Kaolin	$y = 187e^{-0.0279dx}$	$y = 62e^{-0.0228dx}$
Montmorillonite	$y = 162e^{-0.0235dx}$	$y = 58e^{-0.0206dx}$
Graphite: Quartz	$y = 193e^{-0.0206x}$	$y = 151e^{-0.0119x}$
Graphite: Kaolin	$y = 201e^{-0.0249x}$	$y = 156e^{-0.0154x}$
Graphite: Montmorillonite	$y = 193e^{-0.0192x}$	$y = 153e^{-0.0128x}$
Graphite: Montmorillonite: Quartz	$y = 191e^{-0.0196x}$	$y = 152e^{-0.0129x}$
Graphite: Kaolin: Quartz	$y = 195e^{-0.0212x}$	$y = 153e^{-0.0132x}$
Graphite: Montmorillonite: Kaolin	$y = 193e^{-0.0209x}$	$y = 152e^{-0.0127x}$
Graphite: Quartz: Montmorillonite: Kaolin	$y = 190e^{-0.0198x}$	$y = 151e^{-0.0125x}$

attenuation model of mass absorption coefficients of single minerals and composite minerals, a general attenuation model for the grey value of raw coal (composite minerals) can be introduced:

$$G = G_0 e^{\mu_m \rho d} \tag{3}$$

where G_0' — peak grey scale of the background image when the X-ray is unloaded, G' — peak grey scale of the image after X-ray transmission of raw coal (composite minerals), μ_m — mass absorption coefficient of transmissible raw coal (composite minerals), d — thickness of X-rays through raw coal (composite minerals), ρ — density of an object.

In the formula, G_0' and μ_m number is determined, so the grey value of raw coal (composite minerals) under X-ray transmission is only related to the density and thickness, and it can be considered that the grey value of raw coal (composite minerals) has a binary exponential attenuation relationship with the density and thickness. For a certain type of coal, when the density and thickness of the raw coal are determined, its corresponding greyness value is also unique. Therefore, minerals of the same thickness can be classified according to their density.

2.2.3. Establishment of mineral R-values and identification thresholds

R-value can be expressed as the ratio of the greyness peaks in the low-energy and high-energy regions, so the R-value of minerals can be obtained from the greyness peaks of different minerals. R value can be used to distinguish between coal and gangue, mainly because of the different atomic numbers of substances in the X-ray low energy region and high energy region of the attenuation degree of the mass absorption coefficient is different, and with the increase of X-ray intensity, the degree of attenuation of the mass absorption coefficient will be different due to the atomic number of different. As a result, when the atomic number of a substance is low, the difference between its mass absorption coefficient in the high and low energy regions of X-rays is large, and when the atomic number of a substance is high, the difference between its mass absorption coefficient in the high and low energy regions of X-rays is small, which is reflected in the size of the R-value.

The R-value of a single mineral can be obtained according to the peak grey value of different single minerals, as shown in Fig. 10. As can be seen in Fig. 10, graphite R-value range (3.02,3.18), quartz R-value range (2.65,2.72), kaolin R-value range (2.86,2.98), montmorillonite R-value range (2.67,2.77). Graphite has an R-value greater than 3, while the other minerals have R-values less than 3. Therefore, the identification process of coal and gangue can be further analyzed based on the range of R-values of different minerals.

Similar to the R-values of single minerals, the R-values of composite minerals can also be expressed as the ratio of the low-energy region to the high-energy region, as shown in Fig. 11, which shows the R-values of two, three, and four composite minerals obtained from the peak of composite minerals, respectively.

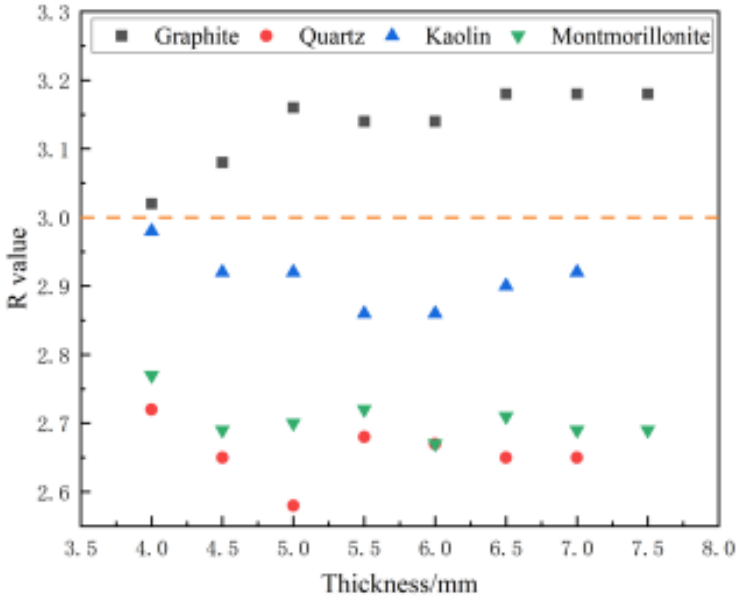

Fig. 10. R-value distribution of four single minerals

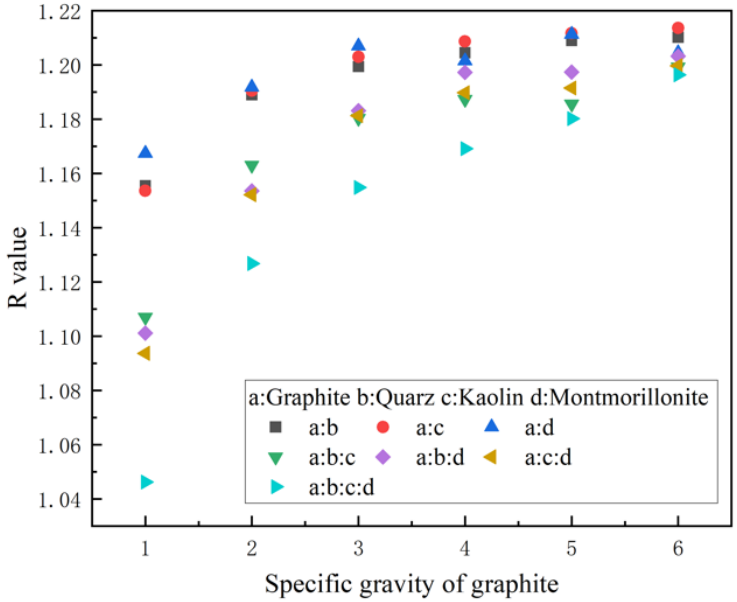

Fig. 11. R-value distribution of four single minerals

As can be seen in Fig. 11, the R-values of the composite minerals range between (1.0,1.3), and the comparison of the R-values of the two composite minerals shows that kaolinite > montmorillonite > quartz, which is in line with the R-values of the single minerals. When the proportion of graphite is fixed, the R-values of the three composite minerals do not change significantly because the composition of graphite in the composite minerals plays a dominant role and because the difference between the R-values of quartz, kaolin and montmorillonite is not large. The R-values of the four composite minerals show a similar relationship to the variation of the single, two and three composite minerals, with the R-values decreasing as the composition of graphite in the composite minerals decreases.

3. Optimization of gangue jet separation mechanism

The research of coal gangue photoelectric sorting technology needs the accurate identification of coal gangue, and at the same time, it is also inseparable from the accurate separation of coal gangue. To achieve accurate separation of coal gangue, while ensuring low energy consumption, it is necessary to optimize the structural parameters of the gangue separation device. Accurate identification of coal

gangue and coal gangue jet separation mechanisms to work together to better achieve the coal gangue photoelectric separation.

3.1. Numerical simulation optimization of nozzle structures

Based on the fluent software simulation analysis of the flow field inside and outside the nozzle, select the nozzle length, the length of the contraction section, the inlet diameter, and the contraction ratio of the variable parameters that have a greater impact on the performance of the nozzle jet, and analyze the impact of each factor on the performance of the nozzle jet from the aspects of the jet velocity, the length of the core section of the jet, and the amount of air consumption to determine the optimal structural parameters of the streamlined nozzle. The single-nozzle velocity variation cloud diagram is shown in Fig. 12.

Gangue jet separation, for large particles of material, requires multiple solenoid valves to act in concert, which requires analyzing the state of the jet produced by multiple nozzles and comparing the appropriate nozzle spacing. The application of array nozzles, the advantage is that multiple jet streams act on the material at the same time, increasing the force area, not needing too high a working air pressure, can meet the separation function, saving energy consumption. The nozzle spacing setting under double nozzle blowing is shown in Table 6.

The double nozzle jet velocity change cloud diagram is shown in Fig. 13. From Fig. 13, it can be found that the jet state and change rule of double nozzles and single nozzles at the exit are the same. At the same time, with the prolongation of the jet time, the two-nozzle flow field appears to merge, forming a flow field with a larger jet cross-section, while the center-axis velocity decreases slowly. The double nozzle pitch velocity graph is shown in Fig. 13.

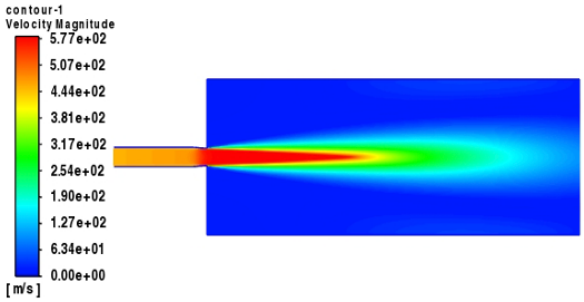

Fig. 12. Single nozzle velocity variation cloud

Table 6. Nozzle spacing setting under dual-nozzle injection

Batch number	1	2	3	4	5
Spacing/mm	14	16	18	20	22

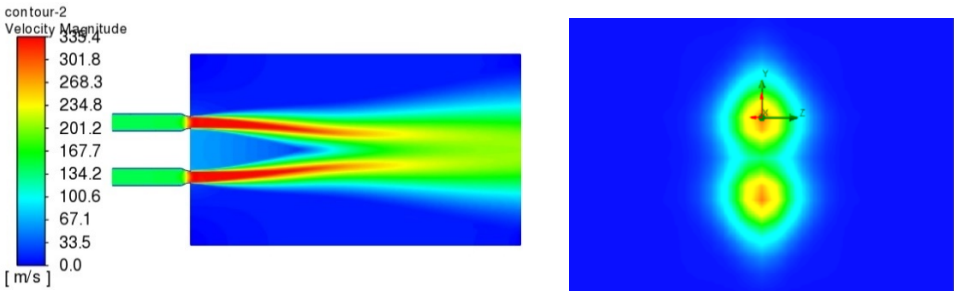

Fig. 13. Cloud image of jet velocity change with 20mm distance between two nozzles

3.2. Analysis of simulation results

3.2.1. Nozzle length

Nozzle lengths of 20 mm, 30 mm, 40 mm, 50 mm, and 60 mm were selected to simulate the effect of nozzle length on jet distribution. Nozzle pairs with different tube lengths are shown in Fig. 14.

From Fig. 14(a), it can be found that the maximum velocity, jet core length, and axial velocity change rule of the nozzle of different tube lengths are approximate, and the velocity of the jet core is about 580 m/s. With the increase of the tube length, the starting position of the jet core is shifted backward, but the total length of the core section remains unchanged. In summary, the total nozzle length has a small effect on the jet velocity and core zone length. From Fig. 14(b), it is found that the air consumption of nozzles with different pipe lengths is similar and does not have a large distinction between them, and the air consumption fluctuates around 0.313 kg/min on average. Therefore, the effect of nozzle length on air consumption is not significant. However, the range pressure loss is directly proportional to the tube length, so reducing the tube length is beneficial to reduce the energy loss.

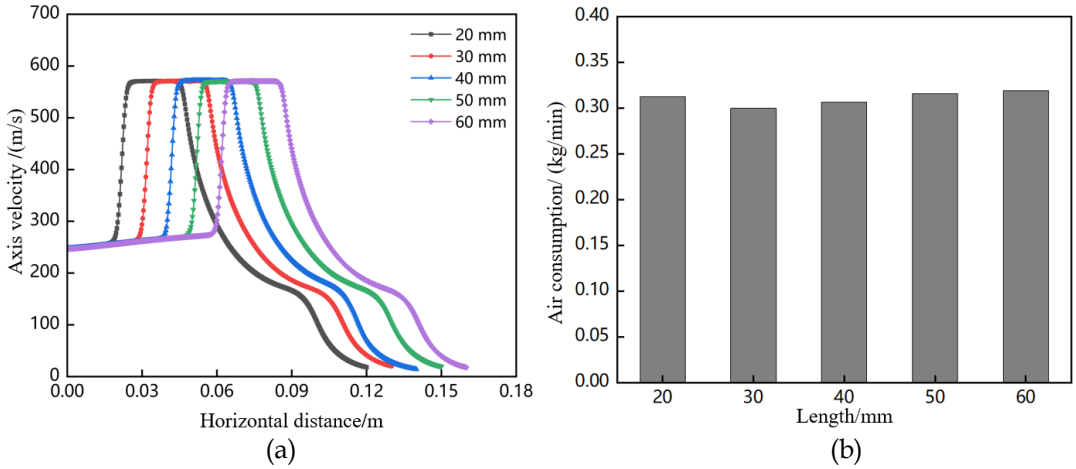

Fig. 14. Comparison of nozzles with different tube lengths. (a) Comparison of axial velocities; (b) Comparison of gas consumption

3.2.2. Inlet diameter

The inlet diameters are selected as 4 mm, 5 mm, 6 mm, 7 mm and 8 mm for simulation. A comparison of nozzles with different inlet diameters is shown in Fig. 15. In Fig. 15(a), with the increase in diameter, the maximum velocity of the nozzles is similar, and the velocities of the core section of the jet are maintained at about 575 m/s, and the length of the core section of the jet is also growing gradually.

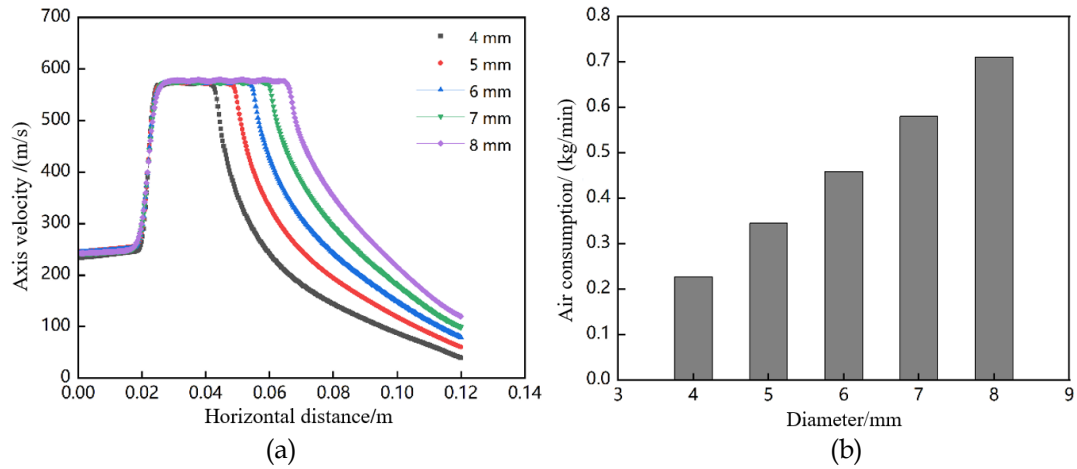

Fig. 15. Comparison of nozzle with different inlet diameters. (a) Comparison of axial velocities; (b) Comparison of gas consumption

The particle size of the sorted material is generally between 20 and 70 mm, and the distance of the nozzle from the sorted material is at least 40 mm, which requires a long enough core section length of the jet. Fig. 15 (b), for the air consumption analysis, found that with the increase in the diameter of the nozzle, air consumption also increases, in the case of the standard core speed and core section length,

the diameter of 8 mm nozzle air consumption is 75% of 5 mm, therefore, from the cost of air consumption and practical applications to analyze the selection of the nozzle inlet diameter of 5 mm.

3.2.3. Shrinkage Segment Length

The length of the shrinkage section is selected as 3 mm, 4 mm, 5 mm, 6 mm, 7 mm. Nozzle comparisons for different shrinkage section lengths are shown in Fig. 16. From Fig. 16(a), it is found that the maximum velocity of jet, core velocity and core length of nozzles with different shrinkage segments are similar, and the shrinkage segment length has less influence on the jet performance. From Fig. 16(b), it is found that when the jet core velocity and core length are similar, the increase in the length of the shrinkage section, the air consumption is also incrementing, so the low air consumption is selected and the nozzle shrinkage section length is 3 mm.

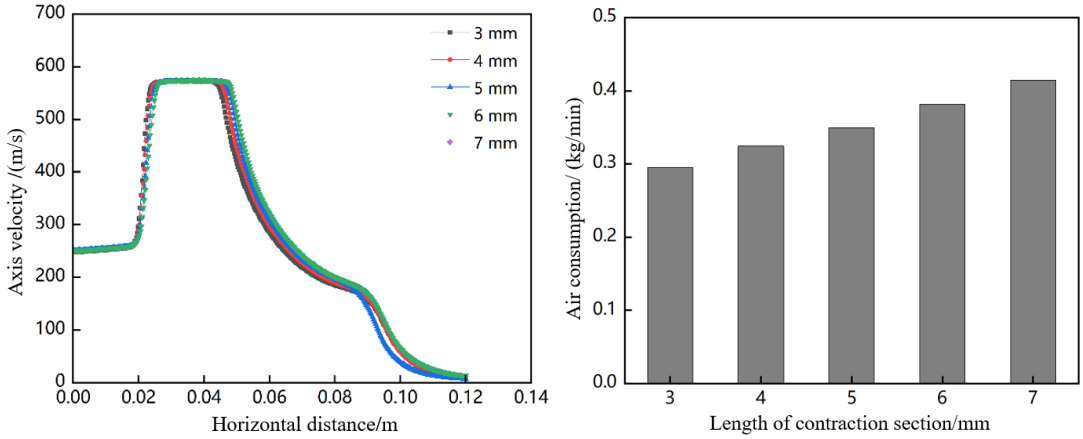

Fig. 16. Comparison of nozzles with different lengths of contraction section. (a) Comparison of axial velocities; (b) Comparison of gas consumption

3.2.4. Systolic ratio

The nozzle shrinkage ratios are set to 1.1, 1.2, 1.3, 1.4 and 1.5 for simulation. Comparison of nozzles with different shrinkage ratios is shown in Fig. 17. From Fig. 17(a), it is found that the nozzle with different shrinkage ratios has little difference in the core velocity of the jet, and the length of the core section of the jet decreases. From Fig. 17 (b), it can be seen that the contraction ratio increases, resulting in decreasing air consumption, the contraction ratio of 1.5 air consumption is the least, the contraction ratio is greater than 1.5, the exit of the nozzle is too small, the material is easy to be deflected by the force.

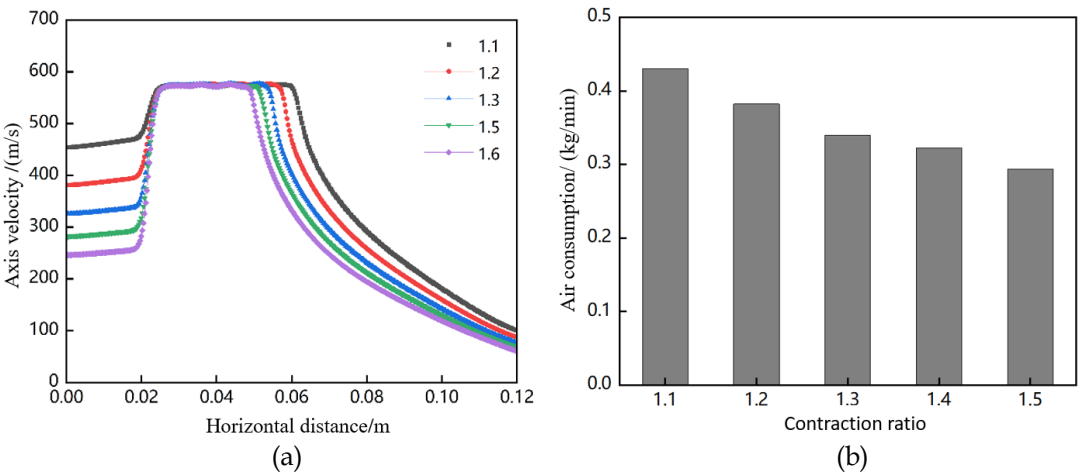

Fig. 17. Comparison of nozzles with different shrinkage ratios. (a) Comparison of axial velocities; (b) Comparison of gas consumption

3.2.5. Multi-nozzle simulation optimization analysis

It can be seen from Fig. 18(a) that the maximum jet axial velocity and the core zone length are similar under different nozzle spacing, compared to the single nozzle independent simulation, the core zone length becomes shorter, and the core zone velocity decreases more significantly. Meanwhile, it can be seen from Fig. 18(b) that the two-nozzle center spacing axial velocity, which rises as the nozzle axial velocity decreases, slowly decreases as the nozzle spacing becomes larger. Explained the double nozzle spacing on the nozzle axial velocity has less impact on the double nozzle center distance axial velocity, the smaller the center distance is the greater the axial velocity of the fusion flow field, the separation of intermediate materials of higher quality. Taking into account the physical properties of the sorting material and the actual assembly of the solenoid valve demand space, the comprehensive consideration of 14 mm. in the spacing of 14 mm, 40 mm away from the nozzle mouth position, out of the longitudinal length of the jet section is about 30 mm, and the take-out ratio will not increase.

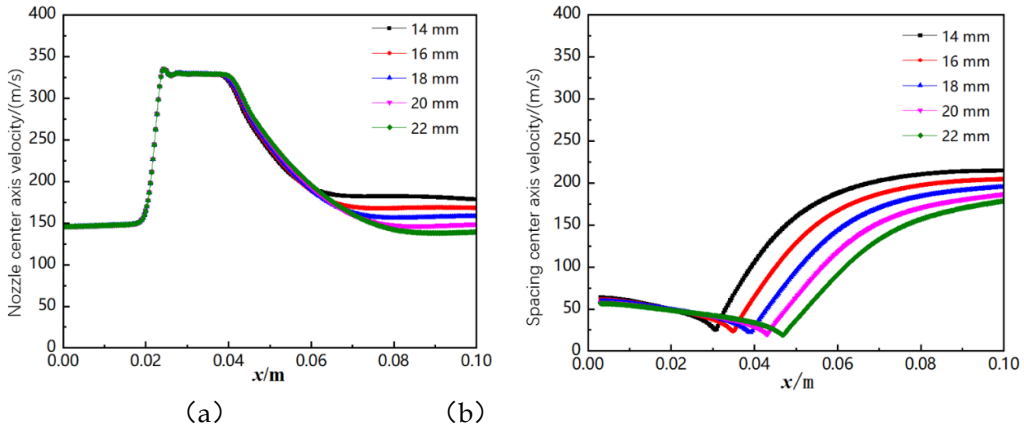

Fig. 18. The velocity curve of the distance between two nozzles(a) Nozzle axis speed; (b) Pitch center axis line speed

4. Conclusions

1. The peak grey levels of single and composite minerals at thickness were derived, exploring a negative correlation between the peak grey levels of composite minerals and thickness. This relationship is independent of the mineral species in the composite minerals, i.e., this empirical equation is satisfied regardless of the composite of several minerals. Comparing the peak grey values of several composite minerals, it is found that an increase in the content of minerals such as quartz, kaolinite, and montmorillonite will make the peak grey value of the composite minerals decrease, which indicates that an increase in clay minerals in coal will make its peak grey value decrease.
2. R-values and identification thresholds were established for single and composite minerals, with graphite R-values ranging from (3.02,3.18), quartz R-values ranging from (2.65,2.72), kaolin R-values ranging from (2.86,2.98), montmorillonite R-values ranging from (2.67,2.77), and composite gangue minerals ranging from (1.0,1.3) between. The R-value identification is reliable based on the difference in identification thresholds for single minerals in coal, especially for graphite versus other clay-based minerals.
3. According to the simulation results of the jet nozzle, several factors affect the jet performance of the streamlined shrinkage nozzle, and the best jet performance is achieved when the total length of the nozzle is 20 mm, the inlet diameter is 5 mm, the shrinkage ratio is 1.5, and the length of the shrinkage section is 3 mm, and the optimal result of the dual-nozzle structure is that the longitudinal length of the outgoing jet cross-section is about 30 mm when the spacing is 14 mm, and the position is 40 mm away from the mouth of the nozzle.

References

DUAN, Y.J., 2010. *Study on variable energy X-ray scanning imaging technology*. North University of China.

GUO, Y.C., HE, L., LIU, P.Z., 2021. *Multi-dimensional analysis and identification method of coal gangue dual-energy X-ray image*. Journal of China Coal Society, 46(01):300-309.2020.1626.

HOU, Z.Y., 2019. *An analysis of the transformation and development of coal utilisation in China*. Contemporary petroleum and petrochemical, 2: 43-47.

HU, B., WANG, S. T., LI, J. Y., 2013. *Experimental study on the nozzle device of automatic identification and sorting machine for waste mixed plastics*. Journal of Tianjin Polytechnic University, 29(01):7-11.

HUANG, S.B., 2018. *40 Years of Reform and Opening Up China's Coal Industry Development Entered the World's Advanced Ranks*. Coal Economic Research, 11: 1.

HUANG, S., WANG, M., ZHANG, J., 2020. *Application analysis of X-ray intelligent gangue separation technology in Yaoqiao coal preparation plant*. Shandong Coal Science and Technology, 8: 186-188.

LIU, W., LIU, C.J., 2018. *The Road of Coal Industry Safety Development in the Past 40 Years of Reform and Opening Up*. Coal Economic Research, 11: 34-42.

ZHAI, R.W., 2019. *Technical analysis of coal preparation based on the concept of energy saving and emission reduction*. Resource conservation and environmental protection, 1: 29.

ZHANG, S.Q., 2016. *Practice and prospect of clean and efficient utilization of coal in China*. Science & Technology Review, 34(17): 56-63.

LI, S.S., 2019. *Analysis of the role of coal preparation in clean coal technology*. Shandong Industrial Technology, (02): 90.

LI, Y.M., ZHANG, Z.H., 1995. *The discovery of X-rays and their impact on modern science and technology*, 8: 474-482.

LI, J., YANG, D., DU, C.,2013. E*valuation of an underground separation device of coal and gangu*e. International Journal of Coal Preparation and Utilization, 33(4): 188-193.

LI, J.P., DU, C.L., XU, L.J., 2011. *Impactive crushing and separation experiment of coal and gangue*. Journal of China Coal Society, 36(4): 687-690.

MA, X.M., JIANG, Y., 2004. *Exploration of digital image processing methods for coal and gangue recognition*. Coal mine electromechanical, 5: 9-11.

MEI, P.L.,2023. *Research on coal gangue identification and detection technology based on deep learning.* China University of Mining and Technology, 2023.002715.

NORLIN B., MANUILSKIY A., NILSSON H.-E., FRÖJDH C., 2004. *Material recognition with the Medipix photon counting colour X-ray system*. Nuclear instruction & Methods in physics research, 531: 265-269.

PAN, Y., ZENG, Z., ZHANG, E.Y., 2017. *A study on gangue identification for X-ray detection based on MATLAB and image grey value*. Coal technology, 36: 307-309.

PICON RUIZ ARTZAI., GHITA OVIDIU., WHELAN PAUL F., IRIONDO PEDRO MARIA., 2010. *Method for integrating spectral and spatial features for classifying materials*.

SONG, X., WANG, G. D., MA, H.,2020. *Mechanism and mathematical modelling of the continuous process of coal breaking by air jets*. Coal Journal, 45(09):3176-3185.

STAŃCZYK K., 2020. M*odelling of Hard Coal Beneficiation Process Utilising Negative Pressure Pneumatic Separator.* Energies, 13(19): 51-74.

YI, T.H., 2022. *Experimental design and analysis*. Machinery Industry Press.

YU, H., YIN, F. F., YAN, L., 2019. *Simulation study of spray and blow separation in plastics near infrared sorting equipment*. Electromechanical engineering, 36(04):378-382.

YUAN, P.X., SUN, L.N., 2006. *Establishment of classification identification curves for substances under dual-energy X-ray transmission conditions*. Journal of Northeastern University (Natural Science Edition), 27: 336-339.